CUS-GS: A Compact Unified Structured Gaussian Splatting Framework for Multimodal Scene Representation

Yuhang Ming¹, Chenxin Fang¹, Xingyuan Yu², Fan Zhang³, Weichen Dai¹,
Wanzeng Kong^{1*}, Guofeng Zhang²

¹School of Computer Science, Hangzhou Dianzi University, ²CAD & CG, Zhejiang University,

³School of Computer Science, University of Bristol

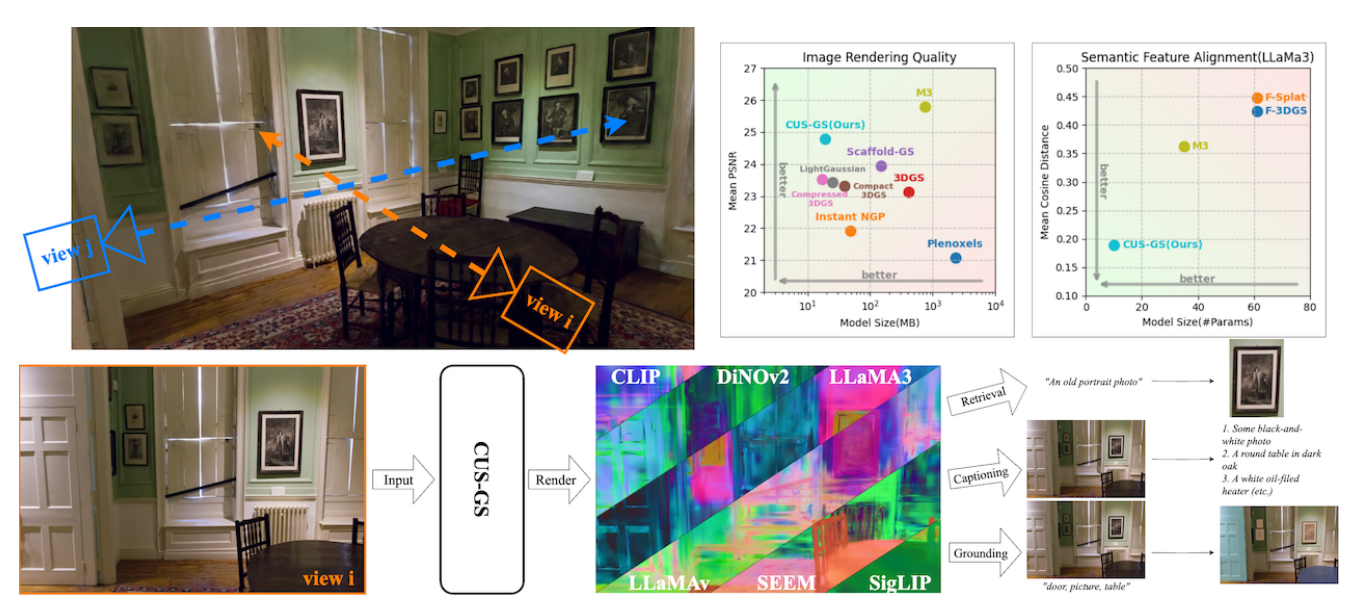


Figure 1. **CUS-GS** is the *first* framework to unify structured 3DGS with multimodal semantic modeling. The voxel-anchored structured design produces a geometry-aware and multimodally aligned 3D feature field, while maintaining high efficiency—achieving competitive performance with as few as 6M parameters, comparing to 35M of the closest rival.

Abstract

Recent advances in Gaussian Splatting based 3D scene representation have shown two major trends: semantics-oriented approaches that focus on high-level understanding but lack explicit 3D geometry modeling, and structure-oriented approaches that capture spatial structures yet provide limited semantic abstraction. To bridge this gap, we present CUS-GS, a compact unified structured Gaussian Splatting representation, which connects multimodal semantic features with structured 3D geometry. Specifically, we design a voxelized anchor structure that constructs a spatial scaffold, while extracting multimodal semantic features from a set of foundation models (e.g., CLIP, DINOv2,

SEEM). Moreover, we introduce a multimodal latent feature allocation mechanism to unify appearance, geometry, and semantics across heterogeneous feature spaces, ensuring a consistent representation across multiple foundation models. Finally, we propose a feature-aware significance evaluation strategy to dynamically guide anchor growing and pruning, effectively removing redundant or invalid anchors while maintaining semantic integrity. Extensive experiments show that CUS-GS achieves competitive performance compared to state-of-the-art methods using as few as 6M parameters — an order of magnitude smaller than the closest rival at 35M — highlighting the excellent trade off between performance and model efficiency of the proposed

1. Introduction

3D scene representation has long been a central topic in computer vision and robotics. As a fundamental module, it bridges perception [29, 33] with various downstream tasks such as 3D reconstruction [22, 61], SLAM [30, 32], navigation [50, 53], and manipulation [36, 57]. In recent years, the community has witnessed remarkable progress in neural rendering–based scene representations (e.g., NeRF [31] and 3DGS [15]), providing a powerful differentiable framework. Among them, 3DGS is particularly promising for its high-fidelity real-time rendering capabilities.

To accommodate different downstream tasks, recent studies on 3DGS-based scene representations have diversified into multiple directions. Among them, two prominent trends are particularly relevant to this work. The first emphasizes structural hierarchy and rendering efficiency, forming the structure-oriented branch. Representative works, such as Scaffold-GS [27] and Octree-GS [42], enhance spatial compactness through voxelization and adaptive spatial subdivision. The second line of research focuses on semantics-oriented extensions, integrating multimodal knowledge and high-level understanding into 3DGS. Examples include Feature 3DGS [63] and M3 [65]. Despite these remarkable advancements, a notable gap still remains between these two paradigms: structure-oriented methods lack semantic understanding capabilities, whereas semantics-oriented methods often compromise spatial consistency and structural regularity.

Targeting this gap, we present CUS-GS (shown in Figure 1), a Compact Unified Structured Gaussian Splatting framework for multimodal 3D scene representation. It aims to endow Gaussian splatting based scene representations with high-level multimodal understanding while maintaining a compact and efficient model structure. In particular, instead of treating structure and semantics as separate objectives, our CUS-GS integrates them within a unified representation that preserves spatial structure while remaining semantically expressive.

To this end, we introduce a structured multimodal scene representation, composed of a 3D voxelized anchor scaffold and a multimodal feature memory. Specifically, we first construct the multimodal memory by extracting features from a set of foundation models and applying redundancy reduction within each feature space. Each voxel anchor maintains a learnable latent feature that governs N 3D Gaussians, which are decoded via a set of shared MLPs to recover their 3D Gaussian attributes and multimodal semantic features. To ensure robust decoding across heterogeneous feature spaces, we design a multimodal latent feature allocation mechanism together with a hierarchical query

adaptation module, enabling a consistent representation of appearance, geometry, and semantics. Finally, we propose a *feature-aware anchor pruning* strategy that enforces compactness by jointly considering the collective significance of the Gaussians governed by each anchor, as well as the capacity and learning dynamics of its latent features. The primary contributions of our proposed CUS-GS are summarized as follows:

- 1. This is the **first attempt** to combine structure and semantics within a **unified**, **compact**, and **efficient** 3DGS framework for **multimodal scene understanding**.
- 2. The novel hierarchical query adaptation mechanism propagates each anchor's latent feature to its associated Gaussian queries through shared MLPs, which significantly reduces the model size (compared to M3 [65] while achieving spatially coherent and semantically adaptive rendering.
- 3. The new **feature-aware anchor pruning strategy** jointly considers the rendering-based significance of the Gaussians governed by each anchor and the capacity and learning dynamics of its latent features, rather than performing pruning based on Gaussian attributes [8, 27] this enables a compact yet semantics-preserving structured representation.

We conduct extensive experiments on several benchmarks to evaluate the performance of our proposed CUS-GS. Results show that CUS-GS achieves competitive image rendering quality and strong multimodal feature alignment across multiple foundation models, while maintaining a model size up to 5× smaller than state-of-the-art methods. Furthermore, experiments on high-level downstream tasks demonstrate that CUS-GS effectively balances semantic consistency, structural fidelity, and model compactness, highlighting its advantage as a unified and efficient multimodal scene representation framework.

2. Related Work

In this section, we review related works on neural rendering-based 3D scene representation. Given the rapid progress and vast literature in this area, we focus on the studies most relevant to our problem setting. We begin with a brief overview of neural rendering-based 3D scene representations, followed by two trending directions: structure-oriented 3DGS and semantic-oriented 3DGS. For a more comprehensive review, readers are referred to existing surveys [1, 2, 26, 33, 48, 49].

Neural Rendering-based Scene Representation: Neural rendering, as the integration of traditional computer graphics and modern deep learning, has established a new paradigm for 3D scene representation [48, 49]. With the emergence of NeRF [31], neural rendering has rapidly become a leading topic in scene representation and re-

lated fields, inspiring a wide range of neural implicit approaches [3, 9, 25, 35, 39, 46]. These methods offer high-fidelity novel view synthesis, but struggle with real-time rendering. To address this limitation, many studies have turned to explicit neural primitives, with 3DGS [15] becoming a central framework. Subsequent work has advanced 3DGS along multiple directions — including expressive capability [5, 55], robustness [16, 54], efficiency [8, 20, 37], and generalizability [60, 62].

Structure-oriented 3DGS: Targeting spatial compactness, a series works have investigated the incorporation of spatial structures and hierarchical organizations. As one of the earliest attempts, Scaffold-GS [27] divides the 3D space into a scaffold of voxels and uses voxel anchors to manage nearby 3D Gaussians. Following this idea, various attempts have been explored to make the spatial distribution of 3D Gaussian more controllable and compact. Examples include 2D grids in self-organizing gaussian grids [34], 3D cubes in GaussianCube [59], octrees in OG-Mapping [51], Octree-GS [42], GS-Octree [24], and hash-grids in HAC [6] and HAC++ [7]. Alternatively, other works such as Hierarchical 3DGS [16], HUG [44], and Virtualized 3D Gaussians [56] organize Gaussians in hierarchical blocks or clusters, enabling level-of-detail rendering for large-scale environments. Meanwhile, RGBDS-SLAM [4], HiSplat [47], HRGS [21], and PyGS [52] construct pyramidal or coarseto-fine hierarchies, supporting multi-scale reconstruction and high-resolution rendering.

Semantic-oriented 3DGS: Aiming to make 3DGS multimodally expressive, a parallel line of works augments 3DGS with semantic features extracted from foundation models. Early approaches distill 2D semantic features from models like CLIP [41], DiNOv2 [38], and SAM [18] into the 3DGS representation, as seen by Feature 3DGS [63], FMGS [66], Semantic Gaussians [11], LEGaussians [43], and Feature-Splat [40]. Concurrently, other works including LUDVIG [28], SLAG [45], and Dr. Splat [14] directly project foundation model features onto the Gaussians, avoiding additional training modules and improving scalability.. In parallel, CLIP-GS [13], UniGS [23], and M3 [65] introduce trainable latent features to each 3D Gaussian and align images, text, and 3D into a shared embedding space.

3. Methodology

3DGS is developing rapidly, with numerous works advancing along two major directions — structure-oriented and semantic-oriented representations. Our approach integrates these two perspectives by constructing a unified structured multimodal representation that jointly encodes spatial layout and multimodal features from six foundation models. The overall architecture of our proposed CUS-GS framework is illustrated in Figure 2. In the follow-

ing, we first briefly review the background of 3DGS and the principal scene components in Sec. 3.1 to make the paper self-contained. We then present our method in detail — Sec. 3.2 introduces the structured multimodal representation, Sec. 3.3 describes the hierarchical query adaptation, Sec. 3.4 explains the feature-aware growing and pruning strategy, and Sec. 3.5 provides training details.

3.1. Preliminaries

3D Gaussian Splatting (3DGS) [15] models a 3D scene using a collection of *spatially independent* anisotropic Gaussian primitives $G_{i=1}^N$. Each Gaussian G_i is parameterized by a mean $\mu_i \in \mathbb{R}^3$, a covariance matrix $\Sigma_i \in \mathbb{R}^{3\times3}$, an opacity $\alpha_i \in [0,1]$, and view-dependent color coefficients c_i modeled by spherical harmonics.

Given a camera projection matrix P, each Gaussian is projected onto the image plane as a 2D Gaussian with mean $\mu'_i = P\mu_i$ and covariance

$$\boldsymbol{\Sigma}_i' = \boldsymbol{J}_i \boldsymbol{\Sigma}_i \boldsymbol{J}_i^{\top}, \tag{1}$$

where J_i denotes the Jacobian of the projection at μ_i . The rendered color at pixel u is then obtained by front-to-back α -compositing of all projected Gaussians:

$$C(\boldsymbol{u}) = \sum_{i=1}^{N} T_i \, \alpha_i \, \boldsymbol{c}_i \, \exp\left(-\frac{1}{2} (\boldsymbol{u} - \boldsymbol{\mu}_i')^{\top} \boldsymbol{\Sigma}_i'^{-1} (\boldsymbol{u} - \boldsymbol{\mu}_i')\right),$$
(2)

where $T_i = \prod_{j < i} (1 - \alpha_j)$ denotes the accumulated transmittance of all previous Gaussians along the ray.

This differentiable rendering formulation allows 3DGS to be optimized end-to-end via standard photometric losses, providing an explicit and efficient representation for high-quality novel view synthesis.

Principal Scene Component (PSC) [65] is a shared multimodal memory bank from multiple foundation models before linking it to 3D Gaussians. Given a set of scene views $\{I_v\}$ and a collection of foundation models $\{\mathcal{F}^j\}_{j=1}^J$, it first extracts dense feature maps from each model and granularity, and flattens them into a set of raw feature vectors

$$\mathcal{R} = \{ \boldsymbol{r}_n \}_{n=1}^{N_{\text{raw}}}, \quad \| \boldsymbol{r}_n \|_2 = 1.$$

To reduce redundancy while preserving the original embedding spaces, PSC applies a similarity-based reduction. In particular, it scans $\mathcal R$ sequentially and selects a vector $\boldsymbol r_n$ as a memory entry if its cosine similarity to all previously selected entries is below a threshold γ . Formally, the resulting multimodal memory bank is

$$\mathcal{M} = \{ oldsymbol{m}_k \}_{k=1}^K \subset \mathcal{R}, \quad ext{s.t.} \ \max_{j < k} \ oldsymbol{m}_k^ op oldsymbol{m}_j < \gamma,$$

where each m_k is directly taken from the original foundation-model features and optionally tagged with its

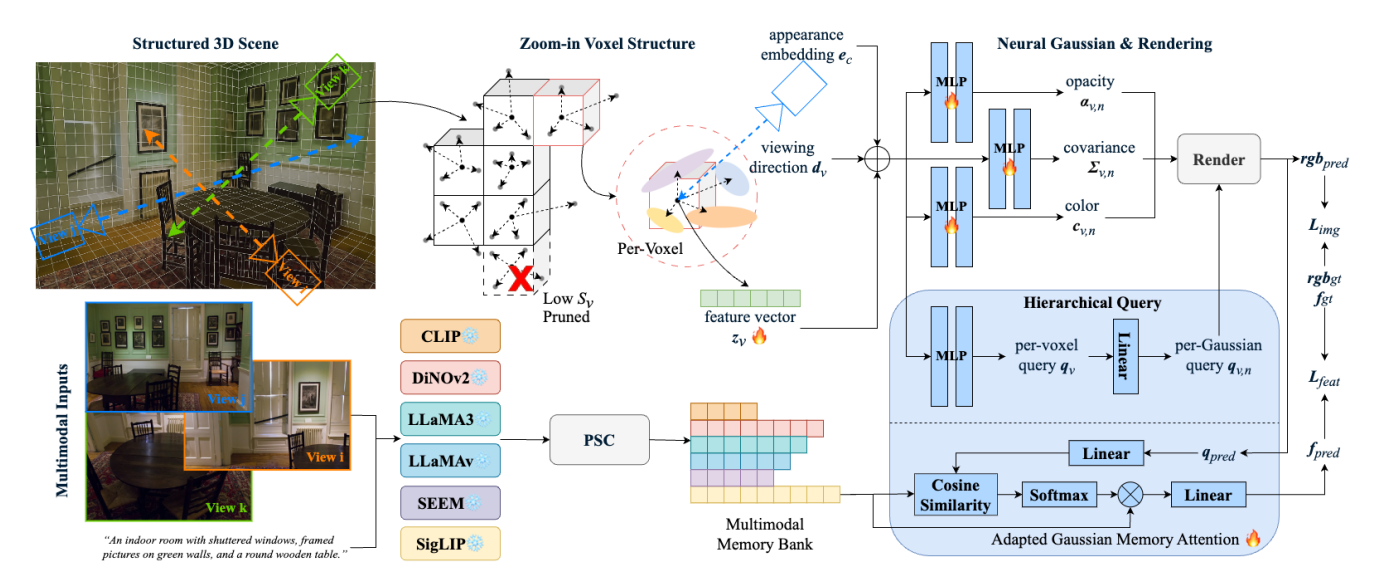


Figure 2. Architecture Overview. Our CUS-GS bridges structured 3DGS with multimodal scene understanding through a voxelized scaffold and a unified multimodal memory bank. Each voxel maintains a latent feature that, together with view-dependent appearance cues, is decoded into hierarchical queries and Gaussian attributess. Multimodal features extracted from 6 foundation models are first compressed via PSC, and are then attended by learned queries to retrieve aligned semantic features. The resulting Gaussian attributes drive differentiable splatting, while the queried semantics enrich the representation, yielding compact, spatially consistent, and multimodally expressive 3D scene representations.

source model and granularity. This memory bank provides a compact yet faithful collection of multimodal scene descriptors, which can later be queried by 3D representations.

3.2. Structured Multimodal Representation

To organize both geometry and multimodal semantics in a unified manner, we divide the 3D space into a voxel scaffold with cell size l. Each voxel v serves as a spatial anchor that governs the attributes of N Gaussian primitives $\{G_{v,n}\}_{n=1}^N$ located within its spatial extent. Following the design philosophy of structural 3DGS methods [6, 7, 27, 42], we associate each voxel with a learnable feature vector $\mathbf{z}_v \in \mathbb{R}^{d_f}$ that jointly encodes its local appearance, geometric, and semantic context, while also interacting with view-related cues to achieve consistent rendering. Specifically, a view-dependent appearance embedding $\mathbf{e}_c \in \mathbb{R}^{d_c}$ is introduced for each camera c to compensate for illumination and tone variations across views, and the voxel's viewing direction \mathbf{d}_v is incorporated to maintain angular coherence.

For each Gaussian inside voxel v, its attributes are decoded from the combination of (z_v, d_v, e_c) through a set of shared lightweight MLPs:

$$\alpha_{v,n} = \text{MLP}_{\text{opacity}}(\boldsymbol{z}_v, \boldsymbol{d}_v, \boldsymbol{e}_c), \tag{3}$$

$$\Sigma_{v,n} = \text{MLP}_{\text{cov}}(\boldsymbol{z}_v, \boldsymbol{d}_v, \boldsymbol{e}_c), \tag{4}$$

$$\boldsymbol{c}_{v,n} = \text{MLP}_{\text{color}}(\boldsymbol{z}_v, \boldsymbol{d}_v, \boldsymbol{e}_c), \tag{5}$$

where each network is shared across all voxels and jointly optimized during training. To maintain spatial flexibility,

each Gaussian's local position is parameterized by a learnable offset $\Delta x_{v,n}$ relative to the voxel center.

In addition to geometric and appearance attributes, we further decode per-Gaussian semantic queries for multimodal reasoning. A separate network F_{θ} maps the same input triplet: (z_v, d_v, e_c) to semantic query vectors:

$$\boldsymbol{q}_{v,n} = F_{\theta}(\boldsymbol{z}_v, \boldsymbol{d}_v, \boldsymbol{e}_c), \tag{6}$$

which serves as the intermediate representation for hierarchical query adaptation and multimodal memory retrieval introduced in Sec. 3.3.

This design allows each voxel to encapsulate local structure and multimodal context, producing a compact and spatially coherent latent scaffold that can be consistently decoded into geometry, appearance, and semantic attributes across views.

3.3. Hierarchical Query Adaptation

We retrieve multimodal semantic features through a query–memory mechanism similar to M3 [65], using PSCs as the memory bank (see Sec. 3.1). However, flat per-Gaussian querying often leads to redundant and spatially inconsistent retrievals, as neighboring Gaussians may correspond to a similar visual context [65]. To overcome this limitation, we introduce a hierarchical adaptation mechanism that propagates multimodal queries from voxel-level anchors to individual Gaussians, ensuring both spatial coherence and semantic adaptability.

Specifically, each voxel feature z_v is first mapped to a voxel-level query $q_v \in \mathbb{R}^{d_q}$ through a lightweight MLP:

$$\boldsymbol{q}_v = \mathrm{MLP}_{qv}(\boldsymbol{z}_v, \boldsymbol{d}_v, \boldsymbol{e}_c), \tag{7}$$

which encodes aggregated appearance, geometric, and multimodal cues within the voxel. For each Gaussian $G_{v,n}$ governed by voxel v, a finer query $q_{v,n} \in \mathbb{R}^{d_q}$ is derived from the voxel query and the Gaussian's relative offset:

$$\mathbf{q}_{v,n} = \operatorname{Linear}_{qg}([\mathbf{q}_v, \Delta \mathbf{x}_{v,n}]),$$
 (8)

where $\Delta x_{v,n}$ denotes the offset. This hierarchical propagation allows local Gaussian queries to inherit the semantic priors of their voxel anchors while capturing position-specific variation.

The per-Gaussian queries are first passed through standard rendering pipeline to obtain predicted queries q_{pred} , which then attend to the multimodal memory bank via dot-product attention in the adapted gaussian memory attention module:

$$a_{pred,k} = \frac{\exp(\boldsymbol{q}_{pred}^{\top} \boldsymbol{m}_k / \sqrt{d})}{\sum_{j} \exp(\boldsymbol{q}_{v,n}^{\top} \boldsymbol{m}_j / \sqrt{d})},$$
 (9)

and the retrieved multimodal feature is obtained by weighted aggregation:

$$\tilde{\boldsymbol{f}}_{pred} = \sum_{k} a_{pred,k} \boldsymbol{m}_{k}. \tag{10}$$

To handle distribution discrepancies among heterogeneous foundation-model features, a linear adaptation layer $\boldsymbol{W}_{\text{adapt}}$ is further applied:

$$\boldsymbol{f}_{pred} = \boldsymbol{W}_{\text{adapt}} \, \tilde{\boldsymbol{f}}_{pred}.$$
 (11)

Through this hierarchical query adaptation, we avoid storing high-dimensional queries for every Gaussian, achieving a more compact representation, while the shared voxel-level queries also encourage smoother semantics across neighboring Gaussians.

3.4. Feature-aware Pruning

To enhance compactness and better exploit voxel-level information, we introduce a feature-aware pruning strategy that evaluates the importance of each voxel using both voxel-feature statistics and Gaussian-attribute indicators.

For voxel-feature statistics, we use two measures: the feature norm $|z_v|^2$, which reflects the magnitude of the learned representation, and the gradient norm $\|\nabla_{z_v}\mathcal{L}\|_2$, which indicates the remaining learning dynamics and thus the potential for further optimization.

For Gaussian-attribute indicators, we compute per-Gaussian contribution score $S_{v,n}^{\text{contrib}}$ following the global significance formulation in [8], which accumulates its hit counts over training rays weighted by opacity and normalized volume. We then aggregate the voxel-level scores as $S_v^{\text{contrib}} = \sum_{n=1}^N S_{v,n}^{\text{contrib}}$.

The final significance score for voxel v is defined as

$$S_v = \lambda_{v,n} \|\boldsymbol{z}_v\|_2 + \lambda_{v,q} \|\nabla_{\boldsymbol{z}_v} \mathcal{L}\|_2 + S_v^{contrib}.$$
 (12)

As voxels with low S_v are pruned, this feature-aware criterion adaptively refines the voxel scaffold by balancing representation strength, learning potential, and rendering contribution.

3.5. Loss Design

The overall training objective combines image reconstruction and multimodal feature alignment losses:

$$\mathcal{L} = \mathcal{L}_{imq} + \lambda_{l,e} \, \mathcal{L}_{feat}. \tag{13}$$

The image reconstruction loss \mathcal{L}_{img} enforces photometric consistency between rendered and ground-truth RGB images, defined as

$$\mathcal{L}_{imq} = \lambda_{l,n} \, \mathcal{L}_{L1} + \lambda_{l,ssim} \, \mathcal{L}_{SSIM} + \lambda_{l,s} \, \mathcal{L}_{scale}, \quad (14)$$

where \mathcal{L}_{L1} and \mathcal{L}_{SSIM} are pixel-wise ℓ_1 and structural similarity losses, respectively, and \mathcal{L}_{scale} is an anchor-scale regularization term to stabilize voxel growth.

The multimodal embedding loss \mathcal{L}_{feat} aligns the reconstructed features with their foundation-model counterparts:

$$\mathcal{L}_{feat} = \mathcal{L}_{\ell_2} + \mathcal{L}_{cos},\tag{15}$$

where \mathcal{L}_{ℓ_2} mmatches feature magnitudes and \mathcal{L}_{cos} enforces directional consistency. This combination ensures faithful RGB reconstruction while maintaining semantic consistency across multimodal embeddings.

4. Experiments

4.1. Experimental Setup

Implementation Details. For the proposed CUS-GS framework, the voxel size is fixed to l=0.01 in all experiments. Each voxel governs N=10 Gaussians, and both the per-voxel feature vector and the per-camera appearance embedding are set to dimension $d_f=d_c=32$. All MLPs consist of two layers with hidden dimensions equal to d_f and ReLU activations. For feature-aware pruning, we remove anchors with the lowest 0.1% importance and set $\lambda_{v,n}=2$ and $\lambda_{v,g}=8$, as validated in the ablation study.

Regarding multimodal semantics, we follow M3 [65] and use a 160 - d query vector to encode features extracted from six foundation models: CLIP [41], SigLIP [58], DI-NOv2 [38], SEEM [64], and LLaMA-3.1/3.2v [10]. We train all models for 30,000 iterations using the Adam

Table 1. Quantitative Comparison on Image Rendering Quality: Our CUS-GS achieves competitive rendering quality with the smallest
multimodal model size, demonstrating the efficiency of our structured multimodal representation.

Method		Mip-NeR	F 360 [3]		-	emple [19]	
Method	Size↓	PSNR↑	SSIM↑	LPIPS↓	Size↓	PSNR↑	SSIM↑	LPIPS↓
Plenoxels [9]	2.1GB	23.08	0.626	0.463	2.3GB	21.08	0.719	0.379
Instant NGP [35]	48MB	25.59	0.699	0.331	48MB	21.92	0.745	0.305
VQ-DVGO [25]	63MB	24.23	0.636	0.393	-	-	-	-
3DGS [15]	734MB	27.21	0.815	0.214	411MB	23.14	0.841	0.183
Scaffold-GS [27]	163MB	28.84	0.848	0.220	148MB	23.96	0.853	0.177
Compact 3DGS [20]	48MB	27.08	0.798	0.247	39MB	23.32	0.831	0.201
Compressed 3DGS [37]	28MB	27.03	0.802	0.238	17MB	23.54	0.838	0.189
LightGaussian [8]	<u>45MB</u>	27.13	0.806	0.237	25MB	23.44	0.832	0.202
M3* [65]	1.1GB	24.14	0.799	0.223	747MB	25.80	0.875	0.171
CUS-GS (Ours)	20MB	26.19	0.822	0.193	<u>19MB</u>	<u>24.79</u>	0.835	0.227

optimizer [17], with the same learning rate schedule as M3 [65], assigning different rates to appearance, geometry, and multimodal parameter groups.

Datasets and Metrics. To evaluate CUS-GS, we conduct experiments on 13 scenes from three public datasets [3, 12, 19]. Following standard practice in 3DGS and multimodal scene representation [8, 27, 65], we adopt the same evaluation protocol as prior studies. Ourbenchmark includes all nine real-world scenes from Mip-NeRF360 [3], (five outdoor and four indoor), the "Train" and "Truck" scenes from the Tank & Temples [19] dataset, and the "Playroom" and "DrJohnson" scenes from DeepBlending [12].

For evaluating imgage rendering quality, we adopt the standard metrics used in novel view synthesis: SSIM, PSNR, and LPIPS. To assess the quality of multimodal semantic features, we evaluate from both low-level feature alignment and high-level downstream task performance perspectives. For low-level feature evaluation, we compute cosine distance and ℓ_2 distance between reconstructed and reference feature maps. For high-level evaluation, following M3 [65] and Feature 3DGS [63], we report mIoU, cIoU, AP50, and AP60 for semantic retrieval with CLIP [41] features, and I2T@1/@5/@10 and T2I@1/@5/@10 for image-text retrieval with SigLIP [58] features. We also report model size for all the experiments, including both checkpoint storage size and total parameter count. All comparison results follow the numbers reported in the original papers; when unavailable, we reproduce them with the authors' official implementations and mark them with an asterisk (*).

Baselines. Since we evaluate our proposed CUS-GS for both image rendering quality and semantic feature alignment, different sets of comparison methods are selected for each task. For color rendering, we include three NeRF-style methods, Plenoxels [9], Instant NGP [35], and VQ-DVGO [25] - as well as five 3DGS-based approaches, Scaffold-GS [27], Compressed 3DGS [37], Com-

pact 3DGS [20], and LightGaussian [8], together with the original 3DGS [15]. For semantic evaluation, we further compare against foundation-model–enhanced 3DGS methods: Feature Splatting (F-Splat) [40], Feature 3DGS (F-3DGS) [63], and M3 [65], with M3 evaluated for both color rendering and multimodal semantics.

4.2. Experimental Results

Quantitative Results. Table 1 presents the quantitative results on image rendering quality. Across all datasets, CUS-GS maintains the smallest model size (20–19 MB), more than an order of magnitude smaller than M3 (1.1 GB) and comparable to the most compact appearance-only 3DGS variants. On the Mip-NeRF360 dataset, our method achieves the best LPIPS (0.193) and the second-highest SSIM (0.822), reflecting strong perceptual and structural fidelity despite a moderate PSNR drop. This trend is consistent with the dataset's diverse, texture-rich scenes, where multimodal supervision provides meaningful regularization and reduces sensitivity to pixel-level noise. On the geometry-dominant Tank and Temples dataset, CUS-GS attains the second-best PSNR (24.79) while retaining competitive SSIM and LPIPS scores, indicating that the model preserves high-quality geometric reconstruction even with multimodal feature integration.

Table 2 summarizes the quantitative comparison on semantic feature alignment. Overall, CUS-GS performs on par with M3 across most foundation models, while showing a clear and consistent improvement on LLaMA3 features. This suggests that the voxel-structured representation and hierarchical query adaptation offer stronger spatial support for language-driven semantic embeddings. A slight decrease is observed for DINOv2, whose texture-oriented and high-frequency visual cues are partially smoothed by voxel-level aggregation. Overall, these results indicate that CUS-GS improves semantic spatial coherence—particularly for high-level, language-oriented representations—without compromising overall multimodal

Table 2. Quantitative Comparison on Semantic Feature Alignment: Our CUS-GS achieves competitive alignment with $5\times$ fewer
parameters. "D." denotes Dataset scenes (T.: Train, G.: Garden, D.: DrJohnson, P.: Playroom), and "# P." the number of parameters.

D.	Method	# P.	DiNO	Ov2	CL	IP	SigI	LIP .	SEI	EM	LLaN	MA3	LLaN	IAv
υ.	Method	# F.	Cosine↓	$\ell_2 \downarrow$										
	F-Splat [40]	61M	0.6833	1.9835	0.5998	0.4779	0.6346	0.7851	0.4269	11.720	0.5300	0.2900	0.7026	56.23
T.	F-3DGS [63]	61M	0.3790	1.0108	0.3330	0.1540	0.3692	0.3328	0.1063	0.1034	0.4993	0.0150	0.6288	46.48
	M3 [65]	35M	0.5321	1.6810	0.3140	0.2800	0.2811	0.5096	0.1389	0.2251	0.4401	0.0253	0.7069	53.43
	CUS-GS (Ours)	13M	0.5515	1.7454	0.3254	0.2871	0.2905	0.5237	0.2036	0.2942	0.2331	0.0251	0.7196	53.56
	F-Splat[40]	61M	0.7328	1.9567	0.7005	1.3570	0.7247	0.8698	0.4224	9.4675	0.4944	0.3314	0.7443	60.83
G.	F-3DGS [63]	61M	0.2295	0.6033	0.2105	0.0945	0.2697	0.2585	0.1071	0.1424	0.4139	0.0141	0.4913	43.08
	M3 [65]	35M	0.5701	1.7279	0.3168	0.2876	0.2927	0.0004	0.1839	0.3469	0.3387	0.0217	0.7235	58.04
	CUS-GS (Ours)	13M	0.6060	1.7991	0.3349	0.2980	0.3056	0.5710	0.1965	0.2817	0.1699	0.0181	0.7374	58.03
	F-Splat [40]	61M	0.8107	2.0333	0.6689	0.7877	0.6826	0.7744	0.4650	10.411	0.3757	0.0145	0.8184	54.82
D.	F-3DGS [63]	61M	0.4190	1.1279	0.3344	0.1537	0.3846	0.3552	0.1693	0.2169	0.3853	0.0150	0.6669	47.35
D.	M3 [65]	35M	0.5878	1.7553	0.3435	0.2924	0.2975	0.5366	0.2456	0.4179	0.3175	0.0226	0.7224	52.68
	CUS-GS (Ours)	8M	0.6063	1.7851	0.3528	0.2987	0.3060	0.5503	0.2063	0.2864	0.1707	0.0182	0.7602	54.18
	F-Splat [40]	61M	0.7956	1.9640	0.6458	0.7808	0.6839	0.7678	0.4745	10.873	0.3915	0.0136	0.8185	59.42
P.	F-3DGS [63]	61M	0.4867	1.2193	0.3813	0.1726	0.4571	0.4094	0.1714	0.2103	0.3987	0.0139	0.6922	52.50
1.	M3 [65]	35M	0.6074	1.7545	0.3260	0.2987	0.2951	0.5623	0.2560	0.4584	0.3555	0.0241	0.7288	57.38
	CUS-GS (Ours)	6M	0.6156	1.7782	0.3345	0.3050	0.3041	0.5718	0.2126	0.2937	0.1810	0.0188	0.7333	57.10

alignment quality.

Table 3 reports the quantitative results on high-level downstream tasks. For CLIP-based semantic segmentation, CUS-GS shows a moderate drop compared with M3 and F-3DGS, which can be attributed both to the reduced model capacity (13–18M vs. 35–61M parameters) and the smoothing inherent to voxel-level aggregation. Because CLIP features contain substantial global context and high-frequency variance, voxel aggregation suppresses local fluctuations and promotes spatial consistency, improving structural coherence while slightly weakening fine-grained semantic discrimination. Nevertheless, CUS-GS maintains competitive segmentation accuracy under a significantly more compact configuration.

For SigLIP-based image—text retrieval, the results exhibit a complementary trend: On the *Train* scene, CUS-GS achieves performance close to the ground truth and clearly surpasses both baselines, indicating strong multimodal grounding in structured environments. In the more cluttered *Playroom* scene, I2T performance decreases whereas T2I metrics remain higher than M3 and F-3DGS. Suggesting that CUS-GS preserves a more stable language-to-vision alignment, even under complex scene layouts.

Overall, these results highlight that CUS-GS achieves a favorable balance between semantic consistency, structural quality, and model compactness, delivering competitive performance with a model size up to 5× smaller than state-of-the-art counterparts.

Qualitative Results. Figure 3 shows qualitative comparisons of multimodal feature maps reconstructed from M3 and our CUS-GS. Overall, CUS-GS produces smoother and more spatially coherent representations. For CLIP and SigLIP, the reconstructed features exhibit more consistent semantic regions, while LLaMA-based features show

clearer spatial organization and improved alignment with scene structure. These observations align well with the quantitative results in Table 2, confirming that the voxel-structured design effectively preserves spatial hierarchy for language-driven semantics. For DINOv2, M3 retains slightly sharper texture cues, whereas CUS-GS appears more smoothed, which corresponds to the minor drop in cosine similarity reported in Table 2. Overall, CUS-GS delivers more stable and spatially consistent multimodal representations across diverse foundation models.

4.3. Ablation Studies

Finally, we conduct three ablation studies in Table 4 to validate key design choices of CUS-GS. The first row reports the results of the *Default Setup*, followed by ablations on *Voxel Size* (rows 2–3), *Query Granularity* (row 4), and *Feature-Awareness Ratio* (rows 5–7).

Voxel Size. As shown in Table 4, the voxel size primarily influences the trade-off between model compactness and rendering quality. A smaller voxel size (0.005) leads to finer details but increases the number of anchors and parameters, while a larger voxel size (0.050) significantly reduces model size at the cost of degraded PSNR. We therefore choose l=0.01 as a balanced configuration that maintains high-quality rendering with moderate memory consumption.

Query Granularity. Switching from per-anchor to per-Gaussian query substantially increases the model size $(13.4M \rightarrow 245.6M)$ with only marginal improvement in rendering quality (PSNR $24.04 \rightarrow 25.27$) and feature alignment. This indicates that hierarchical propagation from voxel anchors is sufficient to capture multimodal semantics without the need for redundant per-Gaussian queries.

Feature-Awareness Ratio. The feature-awareness ratio balances representation magnitude $(\lambda_{v,n})$ and learning dy-

Table 3. **Quantitative Comparison on Downstream Task:** Our CUS-GS achieves comparable downstream performance to M3 with up to $5 \times fewer parameters$, demonstrating strong task generalization under compact model size. "# P." denotes number of parameters.

Dataset	Method	# P.	CLIP				SigLIP					
	Method	# P.	mIoU	cIoU	AP50	AP60	I2T@1	I2T@5	I2T10	T2I@1	T2I@5	T2I@10
Train	Ground Truth	-	25.3	26.3	14.7	3.3	88.7	98.3	100	97.3	100	100
	F-3DGS [63]	61M	24.2	24.3	16.3	7.1	2.6	13.2	28.9	0.0	2.6	18.4
	M3 [65]	35M	25.4	26.5	19.6	12.5	55.2	84.2	92.1	52.6	84.2	92.1
	CUS-GS (Ours)	13M	15.9	16.2	8.4	4.0	85.1	95.0	97.3	77.1	93.7	98.7
Playroom	Ground Truth	-	25.6	24.2	9.6	3.0	92.9	98.7	100	92.0	98.2	98.1
	F-3DGS [63]	61M	23.8	21.4	11.9	3.0	79.3	96.6	6.6	31.0	79.3	89.7
	M3 [65]	35M	23.1	23.1	11.9	5.9	72.4	96.6	100	41.3	65.5	68.9
	CUS-3DGS (Ours)	6M	15.5	16.2	4.8	2.1	37.3	74.2	81.8	58.2	84.8	90.2

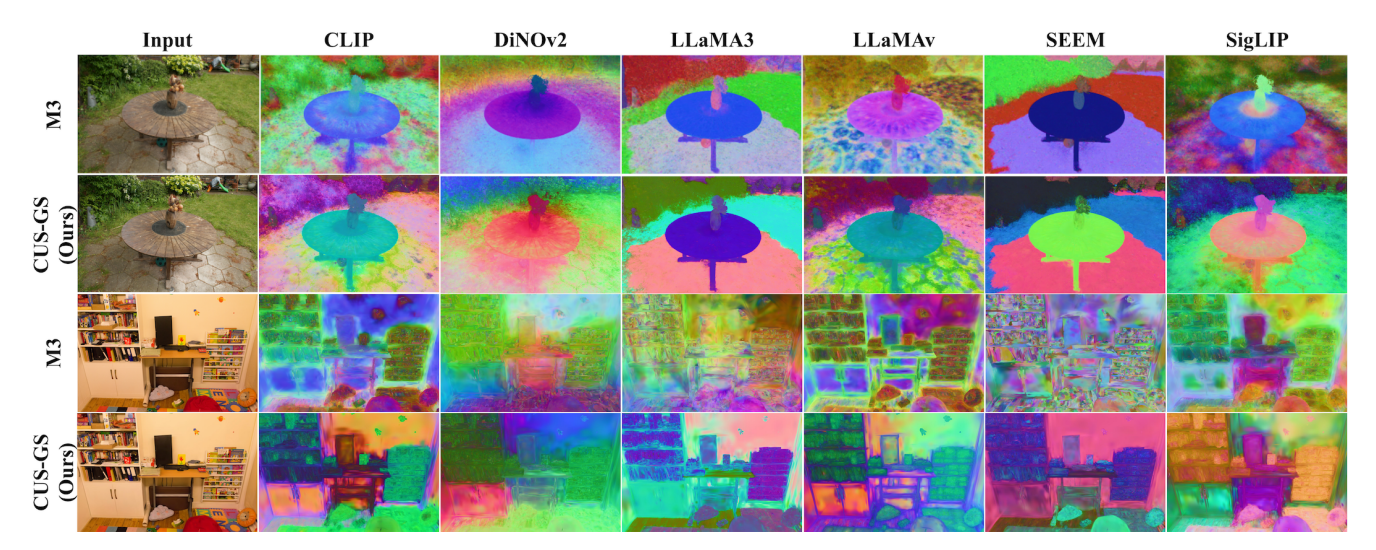


Figure 3. **Qualitative results:** Comparison of example feature maps reconstructed from different foundation models. Our CUS-GS produces smoother and more spatially coherent representations than M3, with clearer structures in language-driven features (e.g., LLaMA3) and slightly smoother texture features (e.g., DINOv2).

namics $(\lambda_{v,g})$ in the pruning process. As shown in rows 5–7 of Table 4, varying the ratio from 8:2 to 4:6 yields only marginal differences in SSIM and PSNR, indicating that the model is robust to moderate weighting changes. Larger $\lambda_{v,n}$ slightly improves PSNR but reduces compactness, while higher $\lambda_{v,g}$ maintains smaller anchor sets with comparable quality. We choose 2:8 as a balanced configuration that provides stable performance and efficient model size.

5. Conclusion

We have presented CUS-GS, the first Compact Unified Structured Gaussian Splatting framework for multimodal 3D scene representation. By bridging structural modeling and multimodal understanding, CUS-GS unifies spatial organization and semantic expressiveness within a single compact architecture. Through voxel-anchored latent features, hierarchical query adaptation, and feature-aware pruning, our method achieves competitive rendering quality and strong multimodal alignment while reducing model size by over 5× compared with existing approaches. Ex-

tensive experiments across diverse benchmarks demonstrate that CUS-GS effectively balances visual fidelity, semantic consistency, and compactness, showing clear advantages for both low-level reconstruction and high-level downstream tasks. We believe this work takes an important step toward unified, scalable, and semantically grounded 3D scene representations, and opens new directions for integrating foundation models into structured 3D learning.

References

- [1] M. T. Bagdasarian, P. Knoll, Y. Li, F. Barthel, A. Hilsmann, P. Eisert, and W. Morgenstern. 3dgs.zip: A survey on 3d gaussian splatting compression methods. *Computer Graphics Forum*, 44(2):e70078, 2025. 2
- [2] Yanqi Bao, Tianyu Ding, Jing Huo, Yaoli Liu, Yuxin Li, Wenbin Li, Yang Gao, and Jiebo Luo. 3d gaussian splatting: Survey, technologies, challenges, and opportunities. *IEEE Transactions on Circuits and Systems for Video Technology*, 35(7):6832–6852, 2025. 2
- [3] Jonathan T. Barron, Ben Mildenhall, Dor Verbin, Pratul P. Srinivasan, and Peter Hedman. Mip-nerf 360: Unbounded

Table 4. Ablation Studies: We analyze the effects of voxel size, query granularity, and feature-awareness (F.A.) ratio on model size, image
rendering quality, and semantic feature alignment.

Dataset		Mode	l Size	RBG	Image	Semantic Features			
	Voxel Size	Query Granularity	F.A. Ratio	#Param	Anchor	SSIM↓	PSNR↓	Avg. Cosine↓	Avg. $\ell_2 \downarrow$
	0.010	per-anchor	2:8	13.4M	128501	0.820	24.04	0.4006	9.4101
	0.050	per-anchor	2:8	8.4M	62639	0.752	23.05	0.4007	9.4114
	0.005	per-anchor	2:8	14.3M	141237	0.815	24.17	0.4006	9.4101
Train	0.010	per-gaussian	2:8	245.6M	150624	0.845	25.27	0.3980	9.3958
114111	0.010	per-anchor	8:2	13.4M	129470	0.818	24.37	0.4006	9.4108
	0.010	per-anchor	6:4	13.4M	128955	0.830	24.79	0.4006	9.4101
	0.010	per-anchor	4:6	13.4M	129465	0.820	24.52	0.4006	9.4105

- anti-aliased neural radiance fields. In 2022 IEEE/CVF Conference on Computer Vision and Pattern Recognition (CVPR), pages 5460–5469, 2022. 3, 6
- [4] Zhenzhong Cao, Chenyang Zhao, Qianyi Zhang, Jinzheng Guang, Yinuo Song, and Jingtai Liu. Rgbds-slam: A rgb-d semantic dense slam based on 3d multi level pyramid gaussian splatting. *IEEE Robotics and Automation Letters*, 10(5): 4778–4785, 2025. 3
- [5] Danpeng Chen, Hai Li, Weicai Ye, Yifan Wang, Weijian Xie, Shangjin Zhai, Nan Wang, Haomin Liu, Hujun Bao, and Guofeng Zhang. Pgsr: Planar-based gaussian splatting for efficient and high-fidelity surface reconstruction. *IEEE Transactions on Visualization and Computer Graphics*, 31 (9):6100–6111, 2025. 3
- [6] Yihang Chen, Qianyi Wu, Weiyao Lin, Mehrtash Harandi, and Jianfei Cai. Hac: Hash-grid assisted context for 3d gaussian splatting compression. In Computer Vision ECCV 2024: 18th European Conference, Milan, Italy, September 29–October 4, 2024, Proceedings, Part VII, page 422–438, Berlin, Heidelberg, 2024. Springer-Verlag. 3, 4
- [7] Yihang Chen, Qianyi Wu, Weiyao Lin, Mehrtash Harandi, and Jianfei Cai. Hac++: Towards 100x compression of 3d gaussian splatting. *IEEE Transactions on Pattern Analysis and Machine Intelligence*, 47(11):10210–10226, 2025. 3, 4
- [8] Zhiwen Fan, Kevin Wang, Kairun Wen, Zehao Zhu, Dejia Xu, and Zhangyang Wang. Lightgaussian: Unbounded 3d gaussian compression with 15x reduction and 200+ FPS. In The Thirty-eighth Annual Conference on Neural Information Processing Systems, 2024. 2, 3, 5, 6, 1
- [9] Sara Fridovich-Keil, Alex Yu, Matthew Tancik, Qinhong Chen, Benjamin Recht, and Angjoo Kanazawa. Plenoxels: Radiance fields without neural networks. In 2022 IEEE/CVF Conference on Computer Vision and Pattern Recognition (CVPR), pages 5491–5500, 2022. 3, 6
- [10] Aaron Grattafiori, Abhimanyu Dubey, Abhinav Jauhri, Abhinav Pandey, et al. The llama 3 herd of models, 2024. 5
- [11] Jun Guo, Xiaojian Ma, Yue Fan, Huaping Liu, and Qing Li. Semantic gaussians: Open-vocabulary scene understanding with 3d gaussian splatting, 2024. 3
- [12] Peter Hedman, Julien Philip, True Price, Jan-Michael Frahm, George Drettakis, and Gabriel Brostow. Deep blending for free-viewpoint image-based rendering. ACM Trans. Graph., 37(6), 2018. 6
- [13] Siyu Jiao, Haoye Dong, Yuyang Yin, Zequn Jie, Yinlong Qian, Yao Zhao, Humphrey Shi, and Yunchao Wei. Clip-

- gs: Unifying vision-language representation with 3d gaussian splatting. In *Proceedings of the IEEE/CVF International Conference on Computer Vision (ICCV)*, pages 4670–4680, 2025. 3
- [14] Kim Jun-Seong, GeonU Kim, Kim Yu-Ji, Yu-Chiang Frank Wang, Jaesung Choe, and Tae-Hyun Oh. Dr. splat: Directly referring 3d gaussian splatting via direct language embedding registration. In 2025 IEEE/CVF Conference on Computer Vision and Pattern Recognition (CVPR), pages 14137– 14146, 2025. 3
- [15] Bernhard Kerbl, Georgios Kopanas, Thomas Leimkuehler, and George Drettakis. 3d gaussian splatting for real-time radiance field rendering. ACM Trans. Graph., 42(4), 2023. 2, 3, 6
- [16] Bernhard Kerbl, Andreas Meuleman, Georgios Kopanas, Michael Wimmer, Alexandre Lanvin, and George Drettakis. A hierarchical 3d gaussian representation for real-time rendering of very large datasets. ACM Trans. Graph., 43(4), 2024. 3
- [17] Diederik P. Kingma and Jimmy Ba. Adam: A method for stochastic optimization. In 3rd International Conference on Learning Representations, ICLR 2015, San Diego, CA, USA, May 7-9, 2015, Conference Track Proceedings, 2015. 6
- [18] Alexander Kirillov, Eric Mintun, Nikhila Ravi, Hanzi Mao, Chloe Rolland, Laura Gustafson, Tete Xiao, Spencer Whitehead, Alexander C. Berg, Wan-Yen Lo, Piotr Dollár, and Ross Girshick. Segment anything. In 2023 IEEE/CVF International Conference on Computer Vision (ICCV), pages 3992–4003, 2023. 3
- [19] Arno Knapitsch, Jaesik Park, Qian-Yi Zhou, and Vladlen Koltun. Tanks and temples: benchmarking large-scale scene reconstruction. ACM Trans. Graph., 36(4), 2017. 6
- [20] Joo Chan Lee, Daniel Rho, Xiangyu Sun, Jong Hwan Ko, and Eunbyung Park. Compact 3d gaussian representation for radiance field. In 2024 IEEE/CVF Conference on Computer Vision and Pattern Recognition (CVPR), pages 21719– 21728, 2024. 3, 6
- [21] Changbai Li, Haodong Zhu, Hanlin Chen, Juan Zhang, Tongfei Chen, Shuo Yang, Shuwei Shao, Wenhao Dong, and Baochang Zhang. Hrgs: Hierarchical gaussian splatting for memory-efficient high-resolution 3d reconstruction, 2025. 3
- [22] Hai Li, Xingrui Yang, Hongjia Zhai, Yuqian Liu, Hujun Bao, and Guofeng Zhang. Vox-surf: Voxel-based implicit surface representation. *IEEE Transactions on Visualization and Computer Graphics*, 30(3):1743–1755, 2024. 2

- [23] Haoyuan Li, Zhou Yanpeng, Tao Tang, Jifei Song, Yihan Zeng, Michael Kampffmeyer, Hang Xu, and Xiaodan Liang. UniGS: Unified language-image-3d pretraining with gaussian splatting. In *The Thirteenth International Conference on Learning Representations*, 2025. 3
- [24] Jiaze Li, Zhengyu Wen, Luo Zhang, Jiangbei Hu, Fei Hou, Zhebin Zhang, and Ying He. Gs-octree: Octree-based 3d gaussian splatting for robust object-level 3d reconstruction under strong lighting, 2024. 3
- [25] Lingzhi Li, Zhen Shen, Zhongshu Wang, Li Shen, and Liefeng Bo. Compressing volumetric radiance fields to 1 mb. In 2023 IEEE/CVF Conference on Computer Vision and Pattern Recognition (CVPR), pages 4222–4231, 2023. 3, 6
- [26] Yun Liao, Yide Di, Hao Zhou, Kaijun Zhu, Mingyu Lu, Qing Duan, and Junhui Liu. A survey on neural radiance fields. *ACM Comput. Surv.*, 58(2), 2025. 2
- [27] Tao Lu, Mulin Yu, Linning Xu, Yuanbo Xiangli, Limin Wang, Dahua Lin, and Bo Dai. Scaffold-gs: Structured 3d gaussians for view-adaptive rendering. In 2024 IEEE/CVF Conference on Computer Vision and Pattern Recognition (CVPR), pages 20654–20664, 2024. 2, 3, 4, 6, 1
- [28] Juliette Marrie, Romain Menegaux, Michael Arbel, Diane Larlus, and Julien Mairal. Ludvig: Learning-free uplifting of 2d visual features to gaussian splatting scenes. In *Proceedings of the IEEE/CVF International Conference on Computer Vision (ICCV)*, pages 7440–7450, 2025. 3
- [29] Ruben Mascaro and Margarita Chli. Scene representations for robotic spatial perception. Annual Review of Control, Robotics, and Autonomous Systems, 8(Volume 8, 2025):351– 377, 2025.
- [30] Hidenobu Matsuki, Riku Murai, Paul H. J. Kelly, and Andrew J. Davison. Gaussian splatting slam. In 2024 IEEE/CVF Conference on Computer Vision and Pattern Recognition (CVPR), pages 18039–18048, 2024. 2
- [31] Ben Mildenhall, Pratul P. Srinivasan, Matthew Tancik, Jonathan T. Barron, Ravi Ramamoorthi, and Ren Ng. Nerf: representing scenes as neural radiance fields for view synthesis. *Commun. ACM*, 65(1):99–106, 2021. 2
- [32] Yuhang Ming, Di Ma, Weichen Dai, Han Yang, Rui Fan, Guofeng Zhang, and Wanzeng Kong. Slc²-slam: Semanticguided loop closure using shared latent code for nerf slam. *IEEE Robotics and Automation Letters*, 10(5):4978–4985, 2025. 2
- [33] Yuhang Ming, Xingrui Yang, Weihan Wang, Zheng Chen, Jinglun Feng, Yifan Xing, and Guofeng Zhang. Benchmarking neural radiance fields for autonomous robots: An overview. *Engineering Applications of Artificial Intelligence*, 140:109685, 2025. 2
- [34] Wieland Morgenstern, Florian Barthel, Anna Hilsmann, and Peter Eisert. Compact 3d scene representation via selforganizing gaussian grids. In Computer Vision – ECCV 2024: 18th European Conference, Milan, Italy, September 29–October 4, 2024, Proceedings, Part LXXXV, page 18–34, Berlin, Heidelberg, 2024. Springer-Verlag. 3
- [35] Thomas Müller, Alex Evans, Christoph Schied, and Alexander Keller. Instant neural graphics primitives with a multiresolution hash encoding. ACM Trans. Graph., 41(4), 2022. 3,

- [36] Suraj Nair, Aravind Rajeswaran, Vikash Kumar, Chelsea Finn, and Abhi Gupta. R3m: A universal visual representation for robot manipulation. In *Conference on Robot Learn*ing, 2022. 2
- [37] Simon Niedermayr, Josef Stumpfegger, and Rüdiger Westermann. Compressed 3d gaussian splatting for accelerated novel view synthesis. In 2024 IEEE/CVF Conference on Computer Vision and Pattern Recognition (CVPR), pages 10349–10358, 2024. 3, 6
- [38] Maxime Oquab, Timothée Darcet, Théo Moutakanni, Huy Vo, et al. Dinov2: Learning robust visual features without supervision, 2024. 3, 5
- [39] Albert Pumarola, Enric Corona, Gerard Pons-Moll, and Francesc Moreno-Noguer. D-nerf: Neural radiance fields for dynamic scenes. In 2021 IEEE/CVF Conference on Computer Vision and Pattern Recognition (CVPR), pages 10313– 10322, 2021. 3
- [40] Ri-Zhao Qiu, Ge Yang, Weijia Zeng, and Xiaolong Wang. Language-driven physics-based scene synthesis and editing via feature splatting. In Computer Vision – ECCV 2024: 18th European Conference, Milan, Italy, September 29–October 4, 2024, Proceedings, Part XLI, page 368–383, Berlin, Heidelberg, 2024. Springer-Verlag. 3, 6, 7
- [41] Alec Radford, Jong Wook Kim, Chris Hallacy, Aditya Ramesh, Gabriel Goh, Sandhini Agarwal, Girish Sastry, Amanda Askell, Pamela Mishkin, Jack Clark, Gretchen Krueger, and Ilya Sutskever. Learning transferable visual models from natural language supervision. In *Proceedings* of the 38th International Conference on Machine Learning, ICML 2021, 18-24 July 2021, Virtual Event, pages 8748– 8763. PMLR, 2021. 3, 5, 6, 1
- [42] Kerui Ren, Lihan Jiang, Tao Lu, Mulin Yu, Linning Xu, Zhangkai Ni, and Bo Dai. Octree-gs: Towards consistent real-time rendering with lod-structured 3d gaussians. *IEEE Transactions on Pattern Analysis and Machine Intelligence*, pages 1–15, 2025. 2, 3, 4
- [43] Jin-Chuan Shi, Miao Wang, Hao-Bin Duan, and Shao-Hua Guan. Language embedded 3d gaussians for open-vocabulary scene understanding. In 2024 IEEE/CVF Conference on Computer Vision and Pattern Recognition (CVPR), pages 5333–5343, 2024. 3
- [44] Mai Su, Zhongtao Wang, Huishan Au, Yilong Li, Xizhe Cao, Chengwei Pan, Yisong Chen, and Guoping Wang. Hug: Hierarchical urban gaussian splatting with block-based reconstruction for large-scale aerial scenes. In *Proceedings of* the IEEE/CVF International Conference on Computer Vision (ICCV), pages 28839–28848, 2025. 3
- [45] Laszlo Szilagyi, Francis Engelmann, and Jeannette Bohg. Slag: Scalable language-augmented gaussian splatting. *IEEE Robotics and Automation Letters*, 10(7):6991–6998, 2025. 3
- [46] Matthew Tancik, Vincent Casser, Xinchen Yan, Sabeek Pradhan, Ben P. Mildenhall, Pratul Srinivasan, Jonathan T. Barron, and Henrik Kretzschmar. Block-nerf: Scalable large scene neural view synthesis. In 2022 IEEE/CVF Conference on Computer Vision and Pattern Recognition (CVPR), pages 8238–8248, 2022. 3

- [47] Shengji Tang, Weicai Ye, Peng Ye, Weihao Lin, Yang Zhou, Tao Chen, and Wanli Ouyang. Hisplat: Hierarchical 3d gaussian splatting for generalizable sparse-view reconstruction. In *The Thirteenth International Conference on Learn*ing Representations, 2025. 3
- [48] A. Tewari, O. Fried, J. Thies, V. Sitzmann, S. Lombardi, K. Sunkavalli, R. Martin-Brualla, T. Simon, J. Saragih, M. Nießner, R. Pandey, S. Fanello, G. Wetzstein, J.-Y. Zhu, C. Theobalt, M. Agrawala, E. Shechtman, D. B Goldman, and M. Zollhöfer. State of the art on neural rendering. *Computer Graphics Forum*, 39(2):701–727, 2020. 2
- [49] A. Tewari, J. Thies, B. Mildenhall, P. Srinivasan, E. Tretschk, W. Yifan, C. Lassner, V. Sitzmann, R. Martin-Brualla, S. Lombardi, T. Simon, C. Theobalt, M. Nießner, J. T. Barron, G. Wetzstein, M. Zollhöfer, and V. Golyanik. Advances in neural rendering. *Computer Graphics Forum*, 41(2):703–735, 2022. 2
- [50] Hanqing Wang, Wenguan Wang, Wei Liang, Caiming Xiong, and Jianbing Shen. Structured scene memory for visionlanguage navigation. In 2021 IEEE/CVF Conference on Computer Vision and Pattern Recognition (CVPR), pages 8451–8460, 2021. 2
- [51] Meng Wang, Junyi Wang, Changqun Xia, Chen Wang, and Yue Qi. Og-mapping: Octree-based structured 3d gaussians for online dense mapping, 2024. 3
- [52] Zipeng Wang and Dan Xu. Pygs: Large-scale scene representation with pyramidal 3d gaussian splatting, 2024. 3
- [53] Zihan Wang, Xiangyang Li, Jiahao Yang, Yeqi Liu, and Shuqiang Jiang. Gridmm: Grid memory map for vision-andlanguage navigation. In 2023 IEEE/CVF International Conference on Computer Vision (ICCV), pages 15579–15590, 2023. 2
- [54] Guanjun Wu, Taoran Yi, Jiemin Fang, Lingxi Xie, Xiaopeng Zhang, Wei Wei, Wenyu Liu, Qi Tian, and Xinggang Wang. 4d gaussian splatting for real-time dynamic scene rendering. In 2024 IEEE/CVF Conference on Computer Vision and Pattern Recognition (CVPR), pages 20310–20320, 2024. 3
- [55] Yusen Xie, Zhenmin Huang, Jianhao Jiao, Dimitrios Kanoulas, and Jun Ma. Unigs: Unified geometry-aware gaussian splatting for multimodal rendering, 2025. 3
- [56] Xijie Yang, Linning Xu, Lihan Jiang, Dahua Lin, and Bo Dai. Virtualized 3d gaussians: Flexible cluster-based level-of-detail system for real-time rendering of composed scenes. In Proceedings of the Special Interest Group on Computer Graphics and Interactive Techniques Conference Conference Papers, New York, NY, USA, 2025. Association for Computing Machinery. 3
- [57] Qiaojun Yu, Xibin Yuan, Yu jiang, Junting Chen, Dongzhe Zheng, Ce Hao, Yang You, Yixing Chen, Yao Mu, Liu Liu, and Cewu Lu. Artgs:3d gaussian splatting for interactive visual-physical modeling and manipulation of articulated objects. In 2025 IEEE/RSJ International Conference on Intelligent Robots and Systems (IROS), 2025. 2
- [58] Xiaohua Zhai, Basil Mustafa, Alexander Kolesnikov, and Lucas Beyer. Sigmoid loss for language image pre-training. In 2023 IEEE/CVF International Conference on Computer Vision (ICCV), pages 11941–11952, 2023. 5, 6, 1

- [59] Bowen Zhang, Yiji Cheng, Jiaolong Yang, Chunyu Wang, Feng Zhao, Yansong Tang, Dong Chen, and Baining Guo. Gaussiancube: A structured and explicit radiance representation for 3d generative modeling. In *The Thirty-eighth Annual Conference on Neural Information Processing Systems*, 2024. 3
- [60] Chuanrui Zhang, Yingshuang Zou, Zhuoling Li, Minmin Yi, and Haoqian Wang. Transplat: Generalizable 3d gaussian splatting from sparse multi-view images with transformers. Proceedings of the AAAI Conference on Artificial Intelligence, 39(9):9869–9877, 2025. 3
- [61] Shuaifeng Zhi, Michael Bloesch, Stefan Leutenegger, and Andrew J. Davison. Scenecode: Monocular dense semantic reconstruction using learned encoded scene representations. In 2019 IEEE/CVF Conference on Computer Vision and Pattern Recognition (CVPR), pages 11768–11777, 2019. 2
- [62] Boyao Zhou, Shunyuan Zheng, Hanzhang Tu, Ruizhi Shao, Boning Liu, Shengping Zhang, Liqiang Nie, and Yebin Liu. Gps-gaussian+: Generalizable pixel-wise 3d gaussian splatting for real-time human-scene rendering from sparse views. *IEEE Transactions on Pattern Analysis and Machine Intelli*gence, pages 1–16, 2025. 3
- [63] Shijie Zhou, Haoran Chang, Sicheng Jiang, Zhiwen Fan, Zehao Zhu, Dejia Xu, Pradyumna Chari, Suya You, Zhangyang Wang, and Achuta Kadambi. Feature 3dgs: Supercharging 3d gaussian splatting to enable distilled feature fields. In 2024 IEEE/CVF Conference on Computer Vision and Pattern Recognition (CVPR), pages 21676–21685, 2024. 2, 3, 6, 7, 8
- [64] Xueyan Zou, Jianwei Yang, Hao Zhang, Feng Li, Linjie Li, Jianfeng Wang, Lijuan Wang, Jianfeng Gao, and Yong Jae Lee. Segment everything everywhere all at once. In *Thirty-seventh Conference on Neural Information Processing Systems*, 2023. 5
- [65] Xueyan Zou, Yuchen Song, Ri-Zhao Qiu, Xuanbin Peng, Jianglong Ye, Sifei Liu, and Xiaolong Wang. 3d-spatial multimodal memory. In *The Thirteenth International Conference* on Learning Representations, 2025. 2, 3, 4, 5, 6, 7, 8, 1
- [66] Xingxing Zuo, Pouya Samangouei, Yunwen Zhou, Yan Di, and Mingyang Li. FMGS: foundation model embedded 3d gaussian splatting for holistic 3d scene understanding. *Int. J. Comput. Vis.*, 133(2):611–627, 2025. 3

CUS-GS: A Compact Unified Structured Gaussian Splatting Framework for Multimodal Scene Representation

Supplementary Material

6. Overview

In this supplementary material, we first provide additional experimental details in Sec. 7. We then include extended qualitative results to further illustrate the capabilities of CUS-GS, including additional image rendering results in Sec. 8, semantic feature rendering comparisons in Sec. 9, and visualizations for downstream tasks in Sec. 10.

7. Additional Experimental Details

In this section, we provide additional details on ground truth generation and evaluation procedure for the quantitative comparison in Table 3. To ensure full consistency with the evaluation protocol of M3 [65], we adopt the same ground-truth construction pipeline for both CLIP [41] segmentation and SigLIP [58] retrieval. Since SoM (semantic-SAM) and GPT-40 used in M3 are not publicly available, we replace them with fully open-source counterparts: SAM for mask generation and Qwen-VL for caption generation. This substitution does not change the mask granularity or the supervision structure, and all feature extraction and evaluation steps remain identical to M3.

For CLIP segmentation, we first apply SAM to the input RGB image to obtain region-level masks, which are then passed through Qwen-VL to obtain natural-language descriptions. During evaluation, the image feature maps are taken from the reconstructed multimodal representation, while the text embeddings are obtained by encoding the region descriptions with the CLIP text encoder. Both features are normalized, and their dot-product similarity is computed to form similarity maps corresponding to each region description. These maps are upsampled to the resolution of the SAM masks and thresholded using Otsu's method to produce predicted regions. We then compare the predictions with the SAM masks to compute mIoU, cIoU, and AP@0.5/0.6.

For SigLIP retrieval, we use Qwen-VL to generate a global caption for the target image, and then extract the image and text embeddings using the SigLIP vision and text encoders. We additionally encode COCO images and their captions with SigLIP to form a negative sample pool, which is combined with the target features to construct the retrieval set. During evaluation, we compute cosine similarities between the target image embedding and all text embeddings to obtain I2T@k, and likewise compute similarities between the target caption embedding and all image embeddings to obtain T2I@k.

8. Image Rendering Results

Figure 4 presents qualitative comparisons of the image rendering results. While the rendered images across different methods appear visually similar at first glance, the residual maps reveal a much clearer distinction. Our CUS-GS consistently produces smaller and more uniformly distributed residuals, indicating more accurate color reconstruction and better alignment with ground-truth imagery. In contrast, both M3 [65] (the only multimodal counterpart) and Light-Gaussian [8] exhibit noticeable structured errors, particularly around object boundaries and high-frequency regions, while Scaffold-GS [27] shows moderate deviations.

9. Semantic Feature Rendering Results

Figure 5 presents additional semantic feature rendering results for the remaining two scenes, "DrJohnson" and "Train," complementing the qualitative comparisons shown in the main text. Across both scenes, CUS-GS consistently produces cleaner and more spatially coherent multimodal features, with CLIP and SigLIP exhibiting more stable semantic regions and LLaMA-based features showing clearer structural organization. As observed previously, DINOv2 features from CUS-GS appear slightly smoother than those from M3, corresponding to the minor alignment trade-off discussed in Table 2. Overall, these additional visualizations further confirm the robustness and spatial consistency of the multimodal representations rendered by CUS-GS.

10. Downstream Tasks Visualization

In this section, we provide additional visualizations for the downstream tasks—retrieval, grounding, and caption—as shown in Figure 6, Figure 7, and Figure 8. These examples illustrate how the multimodal features reconstructed by CUS-GS can be directly used in practical semantic reasoning tasks through the decoders of their corresponding foundation models. The results show that the rendered features remain well aligned with the native feature spaces of these models, enabling them to produce meaningful and coherent outputs without any task-specific adaptation. This further verifies that CUS-GS preserves not only semantic consistency but also functional usability across diverse downstream scenarios.

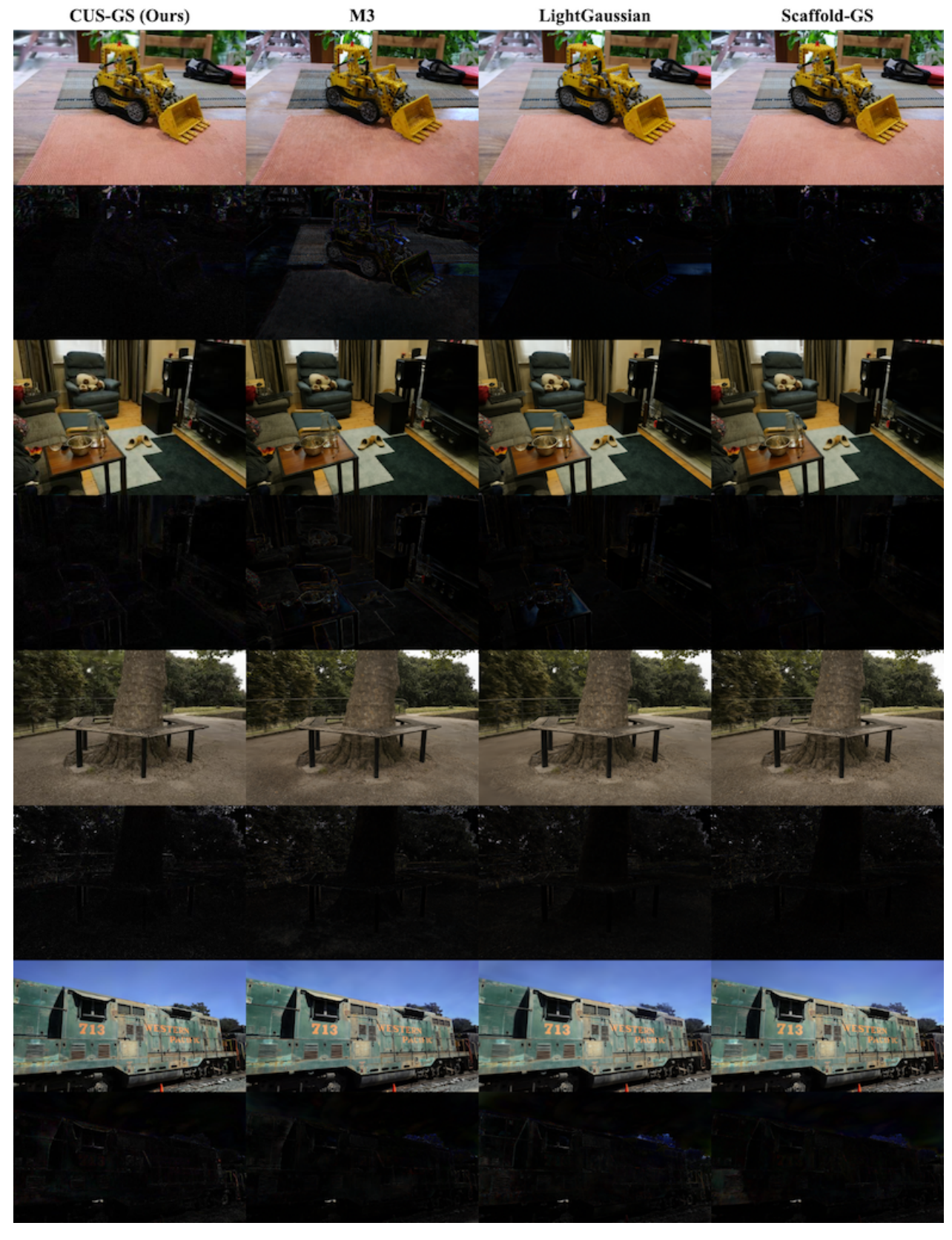


Figure 4. **Examples of the Image Rendering Results.** For each scene, the upper row shows the rendered image, and the lower row presents the residual between the rendered image and the ground truth image.

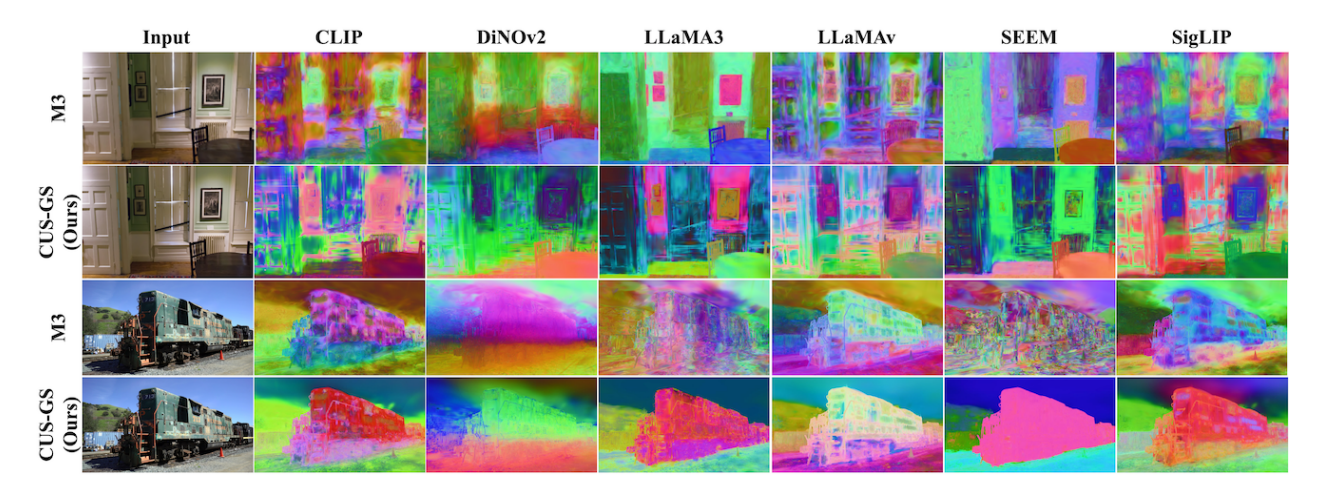


Figure 5. Additional Feature Rendering Results. These results provide complementary evidence that CUS-GS outperforms M3 in producing cleaner and more structured multimodal feature fields.



Figure 6. **Examples of Retrieval Tasks.** Given text queries ("Trash Bin", "Toys", "Ball", "Fire Extinguisher"), we show the top-1 retrievals using CUS-GS's reconstructed features. The top row displays example views from the corresponding scenes, and the bottom row demonstrates the retrieved target, successfully locating the correct object instances.



Figure 7. **Examples of Grounding Tasks.** The upper row shows the input view and text prompt, and the lower row presents the object mask.

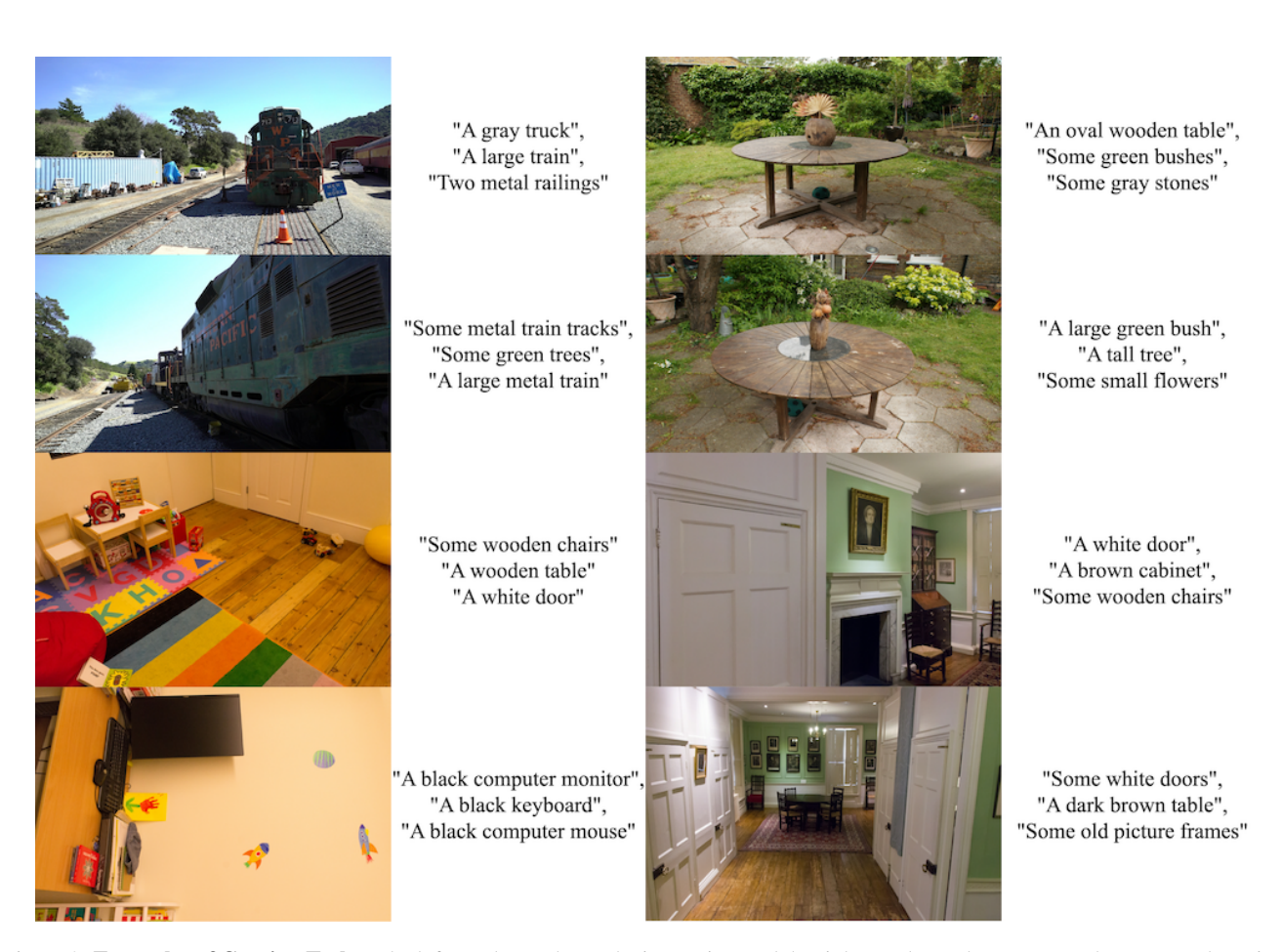


Figure 8. Examples of Caption Tasks. The lefter column shows the input view and the righter column demonstrates the generated caption.